Manuscript submitted to the Journal of the Atmospheric Sciences. The paper is currently under review.

Spontaneous Cyclogenesis without Radiative and Surface-Flux Feedbacks

Argel Ramírez-Reyes (1) and Da Yang* (1, 2)

Affiliations:

1. University of California, Davis
2. Lawrence Berkeley National Laboratory

*Contact information: dayang@ucdavis.edu

Manuscript submitted to the Journal of the Atmospheric Sciences. The paper is currently under review.

Abstract:

Tropical cyclones (TCs) are among the most intense and feared storms in the world. What physical processes lead to cyclogenesis remains the most mysterious aspect of TC physics. Here, we study spontaneous TC genesis using cloud-resolving simulations over an *f*-plane with constant sea-surface temperature. Previous studies proposed that spontaneous TC genesis requires either radiative or surface-flux feedbacks. To test this hypothesis, we perform mechanism-denial experiments, in which we switch off both feedback processes. We find that TCs can self-emerge even without radiative and surface-flux feedbacks. Although these feedbacks accelerate the genesis and impact the size of the TCs, TCs can reach similar intensities as those in the control experiment without these feedbacks. We show that TC genesis is associated with an abrupt increase in the Available Potential Energy (APE) and that convective heating dominates the APE production. Our result suggests that spontaneous TC genesis may result from a cooperative interaction between convection and circulation, and that radiative and surface-flux feedbacks accelerate the process.

1. Introduction

A tropical cyclone (TC) is a rapidly rotating storm system over a tropical ocean. It is often characterized by a center of anomalously low surface pressure, a closed low-level atmospheric circulation, a warm core, and a spiral arrangement of thunderstorms. TCs are among the most intense and feared storms of the world, with torrential rains that can last for O(1 week) and destructive winds that span over O(1000 km). In spite of extensive theoretical developments and the ever-advancing observing capabilities, TC genesis remains as the most mysterious aspect of TC physics [see Emanuel (2018) for a comprehensive review].

Observational studies suggested that TCs often form from a pre-existing mid-level cyclonic vortex (Bartels & Maddox, 1991; Davidson et al., 1990; Laing & Fritsch, 1993; McBride & Zehr, 1981; Velasco & Fritsch, 2012). Recent studies observed that a closed "pouch" associated with a tropical wave protects a region of deep convection from the intrusion of dry air, favoring the formation of a surface-concentrated vortex that then intensifies to TC strength (Dunkerton et al., 2009; Raymond & López Carrillo, 2011; Smith et al., 2015; Z. Wang et al., 2010; Z. Wang, 2012).

Although these studies have provided many insights, the high degree of complexity in the real atmosphere makes it difficult to distinguish what physical processes are essential to TC genesis. Here, idealized modeling studies are ideal complements to the observational studies.

Recent work has shown that TCs can spontaneously develop in rotating radiative-convective equilibrium (RRCE) simulations using both cloud-resolving models (CRMs) and general circulation models (GCMs) (Bretherton et al., 2005; Chavas & Emanuel, 2014; Chavas & Reed, 2019; Held & Zhao, 2008; Khairoutdinov & Emanuel, 2013; Merlis et al., 2016; Merlis & Held, 2019; Muller & Romps, 2018; Nolan, Rappin, et al., 2007; Reed & Chavas, 2015; Shi & Bretherton, 2014; Wing et al., 2016; Zhou et al., 2013). These studies suggest that initial disturbances may help TC genesis in the real atmosphere, but they are *not* essential.

Spontaneous TC genesis is considered as *f*-plane convective self-aggregation. Convective self-aggregation is a phenomenon in which large-scale circulations and convective organization can self-emerge over uniform sea-surface temperatures (SSTs) and boundary conditions (Arnold & Randall, 2015; Bretherton et al., 2005; Muller & Held, 2012; Wing et al., 2018; Yang, 2018a, 2018b, 2019). This process is associated with both increasing moist static energy (MSE) variance and increasing eddy available potential energy (APE). Wing et al. (2016) analyzed the MSE variance budget in spontaneous TC genesis and showed that radiative and surface flux feedbacks help increase MSE variance, consistent with non-rotating self-aggregation processes. In addition, the authors removed the radiative feedback by horizontally homogenizing radiative cooling rates and discovered that spontaneous TC genesis was delayed. Muller and Romps (2018) further showed that removing surface-flux feedbacks significantly delays TC genesis and reduces the TC strength at the mature stage. These mechanism-denial experiments are consistent with the MSE analysis, showing that radiative and surface-flux feedbacks contribute to increase MSE variance, favoring TC genesis. As the MSE variance increase is associated with radiative and surface-flux feedbacks, the MSE analyses seem to suggest that spontaneous TC genesis would not occur in the absence of radiative and surface-flux feedbacks. However, as MSE is quasi-conserved in moist adiabatic processes, the MSE analysis may overlook the role of convection.

Evaporation of water from the ocean surface constitutes the most important source of energy for TCs (Emanuel, 2003, 2018). This energy, later released by condensation of water vapor, is key to TC development and maintenance: Convective heating can generate APE, which can subsequently convert to kinetic energy, providing energy for TC genesis and maintenance (Nolan, Moon, et al., 2007). Generation of APE is associated with the development of a warm core, which is necessary to sustain the vortex in hydrostatic and gradient wind balances. Although an APE-centric framework has been widely used to understand convectively coupled tropical circulations (including non-rotating convective self-aggregation) (Anthes & Johnson, 1968; Emanuel et al., 1994; Kuang, 2008; Nolan, Moon, et al., 2007; Veiga et al., 2008; Yang, 2018a), it has not been applied to understand spontaneous TC genesis. Increases in APE are led by APE production due to convection, radiation, and surface fluxes (*e.g.*, Yang 2018a). Therefore, an analysis of the APE highlights the role of convection, complementing the MSE analysis.

In this paper, we combine the analysis of APE with mechanism-denial CRM simulations to address the question of what processes contribute to the spontaneous TC genesis, and what is the minimum recipe. We describe our research methods in Section 2, present simulation results in Section 3, and expose the APE analysis in Section 4. In section 5 we show the sensitivity of our results to changes of the Coriolis parameter and resolution. We conclude and discuss the implications of our findings in Section 6.

2. Methods

2.1 Model and experiment setup

We perform rotating RCE simulations over an *f*-plane using the System for Atmospheric Modeling, SAM, version 6.10.10 (Khairoutdinov & Randall, 2003). SAM is an anelastic model that has been widely used to study tropical convection, (Bretherton et al., 2005; Khairoutdinov & Emanuel, 2013; Muller & Held, 2012; Wing et al., 2016; Yang, 2018a). The horizontal domain is a doubly periodic rectangle of 1024 km × 1024 km with 4-km resolution. The vertical domain is of 34.8 km, and the resolution is 50 m from z = 0 m to z = 1050 m and increases to 600 m at z = 3000 m. The integration timestep is 10 s but it decreases when needed to prevent numerical instabilities. The radiation scheme is that of CAM3 (Community Atmosphere Model 3); the sub

grid-scale scheme is the default Smagorinsky-type scheme; and the microphysics scheme is the SAM single-moment microphysics. The Coriolis parameter is constant: $f = 4.97 \times 10^{-4}\ \mathrm{s}^{-1}$, which corresponds to 10 times the Coriolis parameter at 20° latitude. The large f helps shrink the horizontal scale of TCs and allows us to simulate a TC in a small domain (Khairoutdinov & Emanuel, 2013). The horizontally averaged wind speed is nudged to zero at all levels and the sea surface temperature is held at 300 K. The diurnal cycle is turned off and the solar constant is set to $424\ \mathrm{W\ m}^{-2}$, which approximates the annual mean insolation in the tropical atmosphere.

We investigate the sensitivity of TC genesis to the removal of radiative and surface-flux feedbacks. In the radiation-moisture feedback, radiative cooling leads to subsidence in the dry area, which promotes more radiative cooling and further dries the atmosphere. We remove this feedback by horizontally homogenizing radiative cooling rate at each vertical level (Muller & Romps, 2018; Wing et al., 2016; Yang, 2018a). As the enthalpy fluxes from the sea-surface to the atmosphere depend on wind speed and enthalpy disequilibrium between the surface and low-level air, the surface-flux feedbacks comprise two competing effects. An enhanced wind speed near the surface promotes enthalpy fluxes from the ocean to the atmosphere, which in turn increases the overturning circulation and enhances surface wind speeds, closing the feedback loop. On the other hand, regions of enhanced surface humidity have a decreased enthalpy disequilibrium. This acts to decrease the surface fluxes, weakening the convection and resulting in a negative feedback. The surface-flux feedbacks are removed by horizontally homogenizing the surface fluxes (Muller & Romps, 2018; Yang, 2018a). We will present three simulations: Control, where the interactive radiation and surface fluxes are not altered; HomoRad, where the radiative feedback is turned off; and HomoRad+HomoSfc where radiative and surface-flux feedbacks are turned off.

To test the sensitivity of the results to changes in resolution, we run additional 100-day simulations with a similar setup but using 2-km horizontal resolution in the Control, HomoRad and HomoRad+HomoSfc configurations, and a 30-day simulation with horizontal resolution of 1 km in the HomoRad+HomoSfc configuration. We also run simulations with a horizontal grid spacing of 2-km and $f = 3 \times 10^{-4}\ \mathrm{s}^{-1}$ and $f = 1 \times 10^{-4}\ \mathrm{s}^{-1}$ in the HomoRad+HomoSfc configuration to explore the sensitivity of the results to the Coriolis parameter.

2.2 TC composite

To characterize basic TC features, we make an "average TC" using the last 100 days of each simulation. We first identify TCs using the departure of surface pressure from its horizontal mean ($P'_{sfc}(x,y,t) = P_{sfc}(x,y,t) - \overline{P_{sfc}}(t)$, where the overbar denotes the horizonal mean). Because the scale of a tropical cyclone is of *O*(500 km), we smooth this pressure anomaly with a moving median filter to reduce the smaller scale features. We use a window size of 20 km for smoothing and our results are robust over different choices of the window sizes. We then search for the local minima of the smoothed pressure anomalies. If these minima are less than -9 hPa, we record them as TCs. This threshold value is slightly different than that in (Cronin & Chavas, 2019) (-5 hPa *vs.* -9 hPa), but the result is not changed significantly by changing the threshold. Having obtained the time and location of the TC centers (the minima of surface pressure perturbation), we then create the TC composite by aligning the centers of the identified TCs and taking the time average only over the time steps with identified TCs. This gives a composite of TC-associated variables, including surface pressure, surface winds, air temperature, and others. We can then obtain the characteristic features of TCs by analyzing their composite.

2.3 Available potential energy

APE is the amount of gravitational potential energy that can be transformed into kinetic energy by lowering the center of mass of the atmosphere (Vallis, 2017). APE is, therefore, an energy reservoir for atmospheric circulations. According to Yang (2018a), APE in an anelastic atmosphere is given by

$$APE = \int_0^z \rho_0(z') \frac{\overline{b^2}}{N^2} dz', \tag{1}$$

where b is buoyancy, $\rho_0(z)$ represents the reference density, N^2 is the Brunt-Väisälä frequency squared (a measure of stratification), z denotes the vertical coordinate and the horizontal bar represents horizontal averaging over the region considered.

To obtain an evolution equation for the APE, we consider the buoyancy equation

$$\partial_t b \; + \; u\partial x \; b \; + \; v\partial_y b \; + \; wN^2 \; = \; S_b, \tag{2}$$

where t is time, u,v and w are the components of the velocity vector and S_b represents buoyancy sources, including convective heating, radiative cooling, and surface fluxes. Using (2), Yang (2018a) obtained an evolution equation for the slowly varying component of the APE:

$$\overbrace{\frac{1}{2}\int_0^z \frac{\rho_0}{N^2}\;\partial_t\overline{\tilde{b}^2}\,dz'}^{\partial_t\widehat{APE}} = \overbrace{\int_0^z \frac{\rho_0}{N^2}\overline{\tilde{b}\widetilde{S_b}}\,dz'}^{Production}\overbrace{-\int_0^z \frac{\rho_0}{N^2}\overline{\tilde{b}\widetilde{u\partial_x b}}\,dz' \;-\int_0^z \frac{\rho_0}{N^2}\overline{\tilde{b}\widetilde{v\partial_y b}}\,dz'}^{Advection} - \overbrace{\int_0^z \rho_0\overline{\tilde{b}\tilde{w}}\,dz'}^{Conversion}, \tag{3}$$

where the first term on the right-hand side is the APE production term, the second and third are the advection terms, and the last term is the conversion to kinetic energy. The tilde represents the slowly varying component associated with TCs. According to Yang (2018a), buoyancy sources are computed by

$$S_b = \; g\frac{S_\theta}{\overline{\theta}} + \; g\frac{\epsilon S_q}{1+\epsilon\,\overline{q}}\;, \tag{4}$$

where θ is potential temperature, q is specific humidity, g is the acceleration of gravity, S_q and S_θ are sources of humidity and heating, respectively, and $\epsilon = \frac{M_{air}}{M_{water}} - 1 = 0.62$.

It is important to note from (3) that the production of APE occurs when the product $bS_b$is positive (when buoyancy and buoyancy sources are positively correlated).

2.4 The Okubo-Weiss parameter

A useful quantity to describe the local rotation in a flow is the Okubo-Weiss parameter, defined as:

$$OW = \left(\frac{\partial u}{\partial x} - \frac{\partial v}{\partial y}\right)^2 + \left(\frac{\partial v}{\partial x} + \frac{\partial u}{\partial y}\right)^2 - \left(\frac{\partial v}{\partial x} - \frac{\partial u}{\partial y}\right)^2 \ ,$$

or $OW = s_n^2 + s_s^2 - \omega^2$, where s_n, s_s, and ω are the normal and shear components of strain, and the relative vorticity of the flow, respectively. This quantity separates the relative importance of strain and vorticity, and it has been used to track the development of vortical regions (e.g. Chang & Oey, 2014; Kilroy et al., 2017). Kilroy et al (2017) showed that a coherent region of decreased OW values at from 850 hPa to 500 hPa precedes the intensification of a low pressure system over land. To test the original location of the vortical regions in our experiments, we compute the Okubo-Weiss parameter at $z = 2$ km. We follow Chang & Oey, (2014) in defining a vortex as a connected region that has a OW value smaller than -0.2 times its spatial standard deviation. The decreased OW value indicates a vorticity-dominated region.

3. Results

TCs self-emerge in all three simulations. Figure 1 shows map views of surface winds, surface pressure, and the OW parameter at day 60 for the Control, HomoRad and HomoRad+HomoSfc experiments. All experiments simulate TC-like structures, featuring areas of low surface pressure, high wind speed, and low OW parameter, with a clearly defined eye region in the center. In the Supplemental Material, Movie S1 shows the time evolution of the same variables after starting from a homogeneous state. In the Control simulation, regions of enhanced wind speed occur after 7 days, and a center of low surface pressure is noticeable in the same region by day 8. This low-pressure center coincides with a connected region of decreased OW parameter at 2 km. By day 10, multiple centers of low pressure, low OW, and high wind speed have emerged. As time evolves, the low-pressure centers become centers of low wind speed surrounded by rapidly rotating wind. We consider at this point that TCs are developed. The multiple TCs in Control merge after 68 days, and a single TC that occupies almost the whole domain lasts for the rest of the simulation. In HomoRad this process is slower: the regions of enhanced wind speeds, and decreased OW appear around day 12, and two clearly defined TCs are developed after 16 days. By day 88, multiple TCs have merged into a domain-wide TC. The genesis process is further delayed in HomoRad+HomoSfc. The region of enhanced wind speeds and low OW can be first observed around day 22, and the first clearly defined TC is developed by day 27. The multiple TCs in this

simulation do not merge into a domain-sized TC. Instead, during the simulated period several TCs appear, dissipate, and reappear.

TCs without radiative and surface-flux feedbacks can reach the same intensity as those in the Control simulation. In Figure 1, it seems that TCs in the HomoRad+HomoSfc simulation would not reach the same intensity as those in the control simulation. This result seems consistent with (Montgomery et al., 2006), who proposed that small-scale convective towers with intense cyclonic vorticity in their cores (vortical hot towers) can emerge as coherent structures, generating a tropical depression in a surface-flux-limited configuration. However, we show that TCs become much stronger in the HomoRad+HomoSfc simulation when we increase the horizontal resolution. Figure 2 shows map views of surface wind speed and surface pressure in the Control, HomoRad and HomoRad+HomoSfc simulations with 2-km × 2-km grid spacing at day 60. We observe TCs in the three experiments, all of which reach a *similar intensity*. When the resolution is further increased to 1-km in HomoRad+HomoSfc, the intensity remains similar to that of the 2-km simulation (see movies), suggesting that the intensity of the TCs converge. In the Supplemental material, movies S2 and S3 show simulations at 2-km resolution of Control, HomoRad and HomoRad+HomoSfc (movie S2) and a simulation at 1-km resolution in the HomoRad+HomoSfc (movie S3). For the rest of our paper, we will focus the analysis on the 4-km simulations, which were integrated for a longer period of time and can generate better TC statistics. Otherwise, the horizontal resolution will be explicitly noted.

The distinct timing of TC genesis between different simulations is clear from Figure 3, which illustrates the time evolution of the maximum surface wind speed, minimum surface pressure and the minimum OW at $z = 2$ km. We identify TC genesis as the period when the surface wind speed increases abruptly. This occurs slightly before the rotation is noticeable in the Movie S1: around day 5 in the Control simulation, day 10 in HomoRad and day 20 in HomoRad+HomoSfc (orange lines in Figure 3), and it occurs slightly before the minimum OW parameter experiences an abrupt increase (green lines in Figure 3). The acceleration of TC genesis by radiative and surface-flux feedbacks is consistent with the results of Muller and Romps (2018), Wing et al. (2016) and Zhang and Emanuel (2016).

TC composites show that the simulated TCs have horizontal and vertical structures that resemble observations of real TCs (Figures 4-6). Figure 4 consists of map views of the composites. The upper panel shows surface wind speed and the lower panel shows surface pressure. TCs in the three simulations are all characterized by a center of quiescent winds collocated with a well-defined eye of minimum surface pressure. TCs in the Control and HomoRad simulations almost fill the entire domain, whereas those in HomoRad+HomoSfc are of a smaller spatial extent.

Figure 5 shows more clearly the radial structure of the surface wind speed (Figure 5a) and the surface pressure (Figure 5b). The surface wind speed has a local minimum at the center of minimum pressure in the three cases, and it increases rapidly outward (Figure 5a). The maximum wind speed is around 20 m s^{-1} at 50 km from the center in Control, 18 m s^{-1} at the same distance from the center in HomoRad, and 10 m s^{-1} at about 40 km from the center in HomoRad+HomoSfc. After reaching the maximum, surface wind speed then decreases with distance from the center, reaching 5 m s^{-1} at 430 km in Control, at around 460 km in HomoRad and at 120 km in HomoRad+HomoSfc. This confirms the smaller horizontal extent of TCs in the HomoRad+HomoSfc simulation. Similarly, the surface pressure has a local minimum in the center of the TC, and it increases with distance (Figure 5b). The local minimum in the center has a surface pressure value of 956 hPa in Control, 960 hPa in HomoRad and 991 hPa in HomoRad+HomoSfc, and the maximum value attained far from the center is 1010 hPa in Control and HomoRad, and 1004 hPa in HomoRad+HomoSfc.

The vertical structures of the simulated TCs also are consistent with realistic TCs. Figure 6 shows vertical cross-sections at $y = 512$ km. Because we built the composite by re-centering each TC, the center of the composite TC coincides with the center of the domain. The tangential wind speed (Figure 6a – Figure 6c) is positive to the right of the TC and negative to the left of the TC, indicating cyclonically rotating wind throughout much of the troposphere. Above this cyclonic wind, we observe tangential wind in the opposite direction in the Control and HomoRad composite TCs (Figure 6a and Figure 6b), but not in HomoRad+HomoSfc (Figure 6c). Additionally, Figures 6a-6c, show a buoyant (warm) core indicated by the contours of maximum temperature

perturbation in the center of each TC. The cyclonically rotating wind as well as the buoyant core extend as far as the tropopause, where radiative cooling rate vanishes. The tropopause appears to be around 16 km in Control and HomoRad and around 13.6 km in HomoRad+HomoSfc.

Positive convective heating anomalies extend from near surface to the tropopause and are collocated with the warm core of the simulated TCs (Fig. 6d-f). Convective heating is not standard output of SAM, which solves the conservation law of MSE. Here we diagnose convective heating from the buoyancy equation: we first calculate left-hand-side terms in (2); we then calculate convective heating as the residual of (2)—the left-hand-side terms minus radiative cooling and surface buoyancy fluxes. The deep heating structure in the troposphere captures latent heat release in convective storms. However, heating anomalies in the stratosphere are likely associated with other small-scale parameterized physics. It is worth noting that there is no convective heating in the eye region in our simulations. Because we horizontally smooth the data to capture large-scale circulations associated with TCs, it appears that convective heating is also present in the eyes of TCs.

Convective heating coincides with positive buoyancy anomalies, suggesting positive APE production due to convection (as observed in section 2.3). To examine further this hypothesis, we now examine the time evolution of APE and APE budgets in the simulations.

4 Evolution of APE in the simulated TCs

TC development is associated with APE evolution. Figure 7a shows the time evolution of the total APE in the domain for the three experiments. In all simulations, the APE grows initially with time (the genesis period) and reaches the first local maximum at the same time as the corresponding surface wind speed does (see Figure 1; around day 15, 25 and 30 for Control, HomoRad and HomoRad+HomoSfc, respectively). This suggests that diagnosing APE evolution may help understand TC genesis.

Figures 7b-7d show the APE budgets. In all simulations, convective heating dominates APE production, whereas the contribution of radiative and surface fluxes is modest. Additionally, the

APE production by convective heating is mainly balanced by its conversion to kinetic energy. These results hold, in particular, for Control and HomoRad, where radiative and surface-flux feedbacks are active. This observation may help explain the occurrence of TCs in HomoRad+HomoSfc after removing radiative and surface-flux feedbacks.

Our results challenge the prevailing theory of spontaneous TC genesis. Previous studies regarded surface-flux or radiative feedbacks as essential ingredients in the spontaneous TC genesis process (Muller & Romps, 2018; Wing et al., 2018). However, we found that TCs can self-emerge without radiative and surface-flux feedbacks (Figures 1 and 2). Additionally, our analysis of APE budgets shows that convective heating dominates APE production (Figure 7).

5 Sensitivity of spontaneous TC genesis the Coriolis parameter and resolution

Occurrence of spontaneous TC genesis depends on the value of the Coriolis parameter. Figure 8 shows the time evolution of the maximum wind speed and minimum surface pressure on the Control and HomoRad experiments at 2-km resolution and $f = 5 \times 10^{-4}\ \mathrm{s}^{-1}$. It also shows three HomoRad+HomoSfc experiments with f taking values of $1 \times 10^{-4}\ \mathrm{s}^{-1}$, $3 \times 10^{-4}\ \mathrm{s}^{-1}$, and $5 \times 10^{-4}\ \mathrm{s}^{-1}$. Spontaneous TC genesis occurs in all cases except for the HomoRad+HomoSfc with $f = 1 \times 10^{-4}\ \mathrm{s}^{-1}$ (see also Movies S2, S4 and S5 in the Supplemental material), where convection remains randomly distributed throughout the simulation period. When spontaneous TC genesis occurs, the intensity of the observed TCs is *similar,* although in the HomoRad+HomoSfc experiments, the maximum wind speed increases more gradually from around day 25 to around day 60, and reaches its maximum value around day 60, whereas in Control and HomoRad, the maximum wind speed reaches its maximum value shortly after TC genesis. Our result is consistent with Muller & Romps (2018), who showed that spontaneous TC genesis does not occur when $f = 1 \times 10^{-4}\ \mathrm{s}^{-1}$. It is important to note that $f = 3 \times 10^{-4}\ \mathrm{s}^{-1}$ is around twice the maximum value of the Coriolis parameter in Earth, so we may not expect spontaneous TC genesis on Earth without radiative and surface-flux feedbacks.

Here, we speculate on potential explanations for the dependence of spontaneous TC genesis to the value of *f*. The spatial scale of TCs is approximately proportional to $1/f$ (Chavas & Emanuel, 2014;

Zhou et al., 2013), so TCs in the simulations with $f = 1 \times 10^{-4}\ \mathrm{s}^{-1}$ would have much larger spatial scales than in the fast-rotating simulations if all other factors are equal. Using the same computing domain, the $f = 1 \times 10^{-4}\ \mathrm{s}^{-1}$ simulation may not be able to accommodate a TC, or their TCs have to be much weaker to be accommodated, which then becomes difficult to detect. Another plausible explanation is that increasing the rotation rate reduces the scale separation between convective organization and the deformation radius, favoring TC genesis (Ooyama, 1982). The deformation radius is roughly the minimum spatial scale that feels the effect of rotation and is often much larger than the scale of convective storms. Increasing rotation rate would reduce the deformation radius and thereby the scale separation between convective storms and the deformation radius. This makes it easier for organized convection to feel the effect of rotation, favoring TC genesis. A detailed investigation of the hypotheses is beyond the scope of this study and is left for future work.

Although in this work we focused on simulations with 4-km resolution, we have also performed HomoRad+HomoSfc simulations with 2-km and 1-km horizontal resolutions to test the sensitivity of our results. We find that when resolution is increased, TCs without radiative and surface-flux feedbacks reach roughly the same intensity as those in the Control experiments (Figures 2 and 8). Furthermore, we find that the results converge: when the resolution is increased to 1-km horizontal grid spacing, the intensity of the TCs in the HomoRad+HomoSfc configuration remains unchanged with respect to that experiment with a 2-km resolution. Therefore, our results are robust to the model resolution.

6 Main findings and implications

This paper, for the first time, shows that spontaneous TC genesis can occur after turning off both radiative and surface-flux feedbacks in *f*-plane CRM simulations. The simulated TCs in all of our experiments have realistic horizontal and vertical structures, and our simulation results are robust to varying horizontal resolutions. This result challenges our previous understanding that spontaneous TC genesis requires either radiative or surface-flux feedbacks (Muller & Romps, 2018; Wing et al., 2018). We then find that high Coriolis parameter favors spontaneous TC genesis.

The minimum *f* that allows TCs to self-emerge in HomoRad+HomoSfc exceeds Earth's Coriolis parameter. Therefore, we would not expect to observe this phenomenon in Earth's tropical atmosphere.

Our results are consistent with the *broadly defined* conditional instability of the second kind (CISK), if we define CISK as a cooperative instability between atmospheric flows and convection that does not require surface-flux or radiative feedbacks (Bretherton, 2003). Conventional CISK studies mainly focused on linear stability analysis or computer simulations with parameterized convection (Montgomery & Smith, 2014; Ooyama, 1982; Smith, 1997). These studies are, therefore, subject to criticisms on assumptions in the representation of dynamics or convection. Their simulated TCs are often with a much smaller spatial scale than that the observed TCs. To the best of our knowledge, this paper presents the first 3D nonlinear CRM simulations that actually show that TC genesis can result from interactions between convection and atmospheric circulations. This result is, therefore, a significant advancement in our understanding of TC genesis.

Can convection drive large-scale circulations in the absence of radiative and surface-flux feedbacks (e.g. Emanuel et al., 1994; Ooyama, 1982)? This is a central question in tropical atmospheric dynamics. This paper and recent research show that cooperative interactions between convection and atmospheric circulations can lead to a wide spectrum of convectively coupled circulations, including convective self-aggregation (Muller & Bony, 2015; Yang, 2018a, 2019), TCs (Montgomery & Smith, 2014; Ooyama, 1982), convectively coupled equatorial waves (Andersen & Kuang, 2008; Kuang, 2008; Mapes, 2000) and the Madden-Julian Oscillation (MJO) (B. Wang et al., 2016; Yang & Ingersoll, 2013, 2014). These studies suggest that convection can indeed drive large-scale circulations without radiative and surface-flux feedbacks.

We use an APE-centric framework (Yang 2018a), which complements the widely used MSE analysis. Our APE analyses show that convective heating coincides with buoyancy anomalies (Figure 6) and dominates APE production during both the genesis and mature stages of TC development (Figure 7). The fact that convection dominates the APE production even in the full-

physics simulation may help explain why spontaneous TC genesis can exist without the radiative and surface-flux feedbacks. It is important to note that we use a "dry" APE framework, which treats convective heating as an external heat source. In future studies, it is desirable to analyze our experiments using "moist" variables, including the MSE and moist APE, which may provide additional insights on the spontaneous TC genesis. Aside from an approach centered in thermodynamics, future work focusing on the dynamics (*e.g.*, analysis of vorticity) of spontaneous TC genesis is necessary. The dynamic and thermodynamic approaches are complementary, and a complete picture of the TC genesis should consider both.

The energy that powers TCs ultimately comes from the ocean (Emanuel, 1986, 2003), which transfers energy to the atmosphere primarily through surface sensible and latent heat fluxes. Our experiments are not exceptions, as the surface energy fluxes are key to sustain a moist convecting atmosphere. However, our experiments show that when radiative or surface-flux feedbacks are not active, convective heating may be capable of producing horizontal pressure perturbations, allowing spontaneous TC genesis to occur.

This paper aims to understand TC genesis by studying it in RRCE. In RRCE simulations, TCs can self-emerge, but this process often takes 10 – 30 days (this work, Emanuel, 2018; Muller & Romps, 2018; Wing et al., 2016). This timescale is long comparing to that of synoptic-scale disturbances in the tropical atmosphere: physical processes leading to TC genesis in RRCE might be less efficient than synoptic-scale weather systems. Therefore, there are likely other physical processes that promote TC genesis in the real atmosphere. In future studies, it would be useful to repeat our simulations using a hierarchy of numerical models, which may include aqua-planet GCMs with uniform SSTs, aqua-planet GCMs with realistic SST distributions, and GCMs with realistic topography and SST distributions. This approach will not only test the robustness of our results but will also help bridge the gap between highly idealized studies and observation-based studies.

Data availability

The data for each figure is publicly accessible at
https://ucdavis.box.com/s/snnzay8h8s1iydb12o6d46lgoac8rhda

Acknowledgments

This work was supported by Laboratory Directed Research and Development (LDRD) funding from Berkeley Lab, provided by the Director, Office of Science, of the U.S. Department of Energy under contract DE-AC02-05CH11231. Argel Ramirez-Reyes' doctoral studies are also supported by Mexico's National Council for Science and Technology (CONACYT) and The University of California Institute for Mexico and the United States (UC Mexus) through the CONACYT-UC Mexus doctoral fellowship. Computational resources used were provided by the Department of Energy's National Energy Research Scientific Computing Center (NERSC) at Lawrence Berkeley National Laboratory. The computational model was kindly provided by M. Khairoutdinov and can be obtained through http://rossby.msrc.sunysb.edu/~marat/SAM.html. We thank T. Cronin, S. D. Seidel and W. Zhou for helpful comments during the early stage of this work, D. Nolan for a helpful discussion at the AGU 2019 fall meeting. We also thank Dr. Montgomery for suggesting the OW analysis.

References

Andersen, J. A., & Kuang, Z. (2008). A Toy Model of the Instability in the Equatorially Trapped Convectively Coupled Waves on the Equatorial Beta Plane. *Journal of the Atmospheric Sciences*, *65*(12), 3736–3757. https://doi.org/10.1175/2008JAS2776.1

Anthes, R. A., & Johnson, D. R. (1968). Generation of available potential energy in hurricane hilda (1964). *Monthly Weather Review*, *96*(5), 291–302. https://doi.org/10.1175/1520-0493(1968)096<0291:GOAPEI>2.0.CO;2

Arnold, N. P., & Randall, D. A. (2015). Global-scale convective aggregation: Implications for the Madden-Julian Oscillation. *Journal of Advances in Modeling Earth Systems*, *7*(4), 1499–1518. https://doi.org/10.1002/2015MS000498

Bartels, D. L., & Maddox, R. A. (1991). Midlevel Cyclonic Vortices Generated by Mesoscale Convective Systems. *Monthly Weather Review*, *119*(1), 104–118. https://doi.org/10.1175/1520-0493(1991)119<0104:MCVGBM>2.0.CO;2

Bretherton, C. S. (2003). INSTABILITY | Wave-CISK. In J. R. Holton (Ed.), *Encyclopedia of Atmospheric Sciences* (pp. 1019–1022). Oxford: Academic Press. https://doi.org/10.1016/B0-12-227090-8/00177-9

Bretherton, C. S., Blossey, P. N., & Khairoutdinov, M. F. (2005). An Energy-Balance Analysis of Deep Convective Self-Aggregation above Uniform SST. *Journal of the Atmospheric Sciences*, *62*(12), 4273–4292. https://doi.org/10.1175/JAS3614.1

Chang, Y.-L., & Oey, L.-Y. (2014). Analysis of STCC eddies using the Okubo–Weiss parameter on model and satellite data. *Ocean Dynamics*, *64*(2), 259–271. https://doi.org/10.1007/s10236-013-0680-7

Chavas, D. R., & Emanuel, K. A. (2014). Equilibrium Tropical Cyclone Size in an Idealized State of Axisymmetric Radiative–Convective Equilibrium. *Journal of the Atmospheric Sciences*, *71*(5), 1663–1680. https://doi.org/10.1175/JAS-D-13-0155.1

Chavas, D. R., & Reed, K. A. (2019). Dynamical Aquaplanet Experiments with Uniform Thermal Forcing: System Dynamics and Implications for Tropical Cyclone Genesis and Size. *Journal of the Atmospheric Sciences*, *76*(8), 2257–2274. https://doi.org/10.1175/JAS-D-19-0001.1

Cronin, T. W., & Chavas, D. R. (2019). Dry and semi-dry tropical cyclones. *Journal of the Atmospheric Sciences*. https://doi.org/10.1175/JAS-D-18-0357.1

Davidson, N. E., Holland, G. J., McBride, J. L., & Keenan, T. D. (1990). On the Formation of AMEX Tropical Cyclones Irma and Jason. *Monthly Weather Review*, *118*(10), 1981–2000. https://doi.org/10.1175/1520-0493(1990)118<1981:OTFOAT>2.0.CO;2

Dunkerton, T. J., Montgomery, M. T., & Wang, Z. (2009). Tropical cyclogenesis in a tropical wave critical layer: easterly waves. *Atmos. Chem. Phys.*, 61.

Emanuel, K. A. (1986). An Air-Sea Interaction Theory for Tropical Cyclones. Part I: Steady-State Maintenance. *Journal of the Atmospheric Sciences*, *43*(6), 585–605. https://doi.org/10.1175/1520-0469(1986)043<0585:AASITF>2.0.CO;2

Emanuel, K. A. (2003). Tropical Cyclones. *Annual Review of Earth and Planetary Sciences*, *31*(1), 75–104. https://doi.org/10.1146/annurev.earth.31.100901.141259

Emanuel, K. A. (2018). 100 Years of Progress in Tropical Cyclone Research. *Meteorological Monographs*, *59*, 15.1-15.68. https://doi.org/10.1175/AMSMONOGRAPHS-D-18-0016.1

Emanuel, K. A., Neelin, J. D., & Bretherton, C. S. (1994). On large-scale circulations in convecting atmospheres. *Quarterly Journal of the Royal Meteorological Society*, *120*(519), 1111–1143. https://doi.org/10.1002/qj.49712051902

Held, I. M., & Zhao, M. (2008). Horizontally Homogeneous Rotating Radiative–Convective Equilibria at GCM Resolution. *Journal of the Atmospheric Sciences*, *65*(6), 2003–2013. https://doi.org/10.1175/2007JAS2604.1

Khairoutdinov, M. F., & Emanuel, K. A. (2013). Rotating radiative-convective equilibrium simulated by a cloud-resolving model. *Journal of Advances in Modeling Earth Systems*, *5*(4), 816–825. https://doi.org/10.1002/2013MS000253

Khairoutdinov, M. F., & Randall, D. A. (2003). Cloud Resolving Modeling of the ARM Summer 1997 IOP: Model Formulation, Results, Uncertainties, and Sensitivities. *Journal of the Atmospheric Sciences*, *60*(4), 607–625. https://doi.org/10.1175/1520-0469(2003)060<0607:CRMOTA>2.0.CO;2

Kilroy, G., Smith, R. K., & Montgomery, M. T. (2017). Tropical low formation and intensification over land as seen in ECMWF analyses. *Quarterly Journal of the Royal Meteorological Society*, *143*(703), 772–784. https://doi.org/10.1002/qj.2963

Kuang, Z. (2008). Modeling the Interaction between Cumulus Convection and Linear Gravity Waves Using a Limited-Domain Cloud System–Resolving Model. *Journal of the Atmospheric Sciences*, *65*(2), 576–591. https://doi.org/10.1175/2007JAS2399.1

Laing, A. G., & Fritsch, J. M. (1993). Mesoscale Convective Complexes over the Indian Monsoon Region. *Journal of Climate*, *6*(5), 911–919. https://doi.org/10.1175/1520-0442(1993)006<0911:MCCOTI>2.0.CO;2

Mapes, B. E. (2000). Convective Inhibition, Subgrid-Scale Triggering Energy, and Stratiform Instability in a Toy Tropical Wave Model. *Journal of the Atmospheric Sciences*, *57*(10), 1515–1535. https://doi.org/10.1175/1520-0469(2000)057<1515:CISSTE>2.0.CO;2

McBride, J. L., & Zehr, R. (1981). Observational Analysis of Tropical Cyclone Formation. Part II: Comparison of Non-Developing versus Developing Systems. *Journal of the Atmospheric Sciences*, *38*(6), 1132–1151. https://doi.org/10.1175/1520-0469(1981)038<1132:OAOTCF>2.0.CO;2

Merlis, T. M., & Held, I. M. (2019). Aquaplanet Simulations of Tropical Cyclones. *Current Climate Change Reports*, *5*(3), 185–195. https://doi.org/10.1007/s40641-019-00133-y

Merlis, T. M., Zhou, W., Held, I. M., & Zhao, M. (2016). Surface temperature dependence of tropical cyclone-permitting simulations in a spherical model with uniform thermal forcing. *Geophysical Research Letters*, *43*(6), 2859–2865. https://doi.org/10.1002/2016GL067730

Montgomery, M. T., & Smith, R. (2014). Paradigms for tropical cyclone intensification. *Australian Meteorological and Oceanographic Journal*, *64*(1), 37–66. https://doi.org/10.22499/2.6401.005

Montgomery, M. T., Nicholls, M. E., Cram, T. A., & Saunders, A. B. (2006). A Vortical Hot Tower Route to Tropical Cyclogenesis. *Journal of the Atmospheric Sciences*, *63*(1), 355–386. https://doi.org/10.1175/JAS3604.1

Muller, C. J., & Bony, S. (2015). What favors convective aggregation and why? *Geophysical Research Letters*, *42*(13), 5626–5634. https://doi.org/10.1002/2015GL064260

Muller, C. J., & Held, I. M. (2012). Detailed Investigation of the Self-Aggregation of Convection in Cloud-Resolving Simulations. *Journal of the Atmospheric Sciences*, *69*(8), 2551–2565. https://doi.org/10.1175/JAS-D-11-0257.1

Muller, C. J., & Romps, D. M. (2018). Acceleration of tropical cyclogenesis by self-aggregation feedbacks. *Proceedings of the National Academy of Sciences*, *115*(12), 2930–2935. https://doi.org/10.1073/pnas.1719967115

Nolan, D. S., Rappin, E. D., & Emanuel, K. A. (2007). Tropical cyclogenesis sensitivity to environmental parameters in radiative–convective equilibrium. *Quarterly Journal of the Royal Meteorological Society*, *133*(629), 2085–2107. https://doi.org/10.1002/qj.170

Nolan, D. S., Moon, Y., & Stern, D. P. (2007). Tropical Cyclone Intensification from Asymmetric Convection: Energetics and Efficiency. *Journal of the Atmospheric Sciences*, *64*(10), 3377–3405. https://doi.org/10.1175/JAS3988.1

Ooyama, K. V. (1982). Conceptual Evolution of the Theory and Modeling of the Tropical Cyclone. *Journal of the Meteorological Society of Japan. Ser. II*, *60*(1), 369–380. https://doi.org/10.2151/jmsj1965.60.1_369

Raymond, D. J., & López Carrillo, C. (2011). The vorticity budget of developing typhoon Nuri (2008). *Atmospheric Chemistry and Physics*, *11*(1), 147–163. https://doi.org/10.5194/acp-11-147-2011

Reed, K. A., & Chavas, D. R. (2015). Uniformly rotating global radiative-convective equilibrium in the Community Atmosphere Model, version 5. *Journal of Advances in Modeling Earth Systems*, *7*(4), 1938–1955. https://doi.org/10.1002/2015MS000519

Shi, X., & Bretherton, C. S. (2014). Large-scale character of an atmosphere in rotating radiative-convective equilibrium. *Journal of Advances in Modeling Earth Systems*, *6*(3), 616–629. https://doi.org/10.1002/2014MS000342

Smith, R. K. (1997). On the theory of cisk. *Quarterly Journal of the Royal Meteorological Society*, *123*(538), 407–418. https://doi.org/10.1002/qj.49712353808

Smith, R. K., Montgomery, M. T., Kilroy, G., Tang, S., & Müller, S. K. (2015). Tropical low formation during the Australian monsoon: the events of January 2013, 25.

Vallis, G. K. (2017). *Atmospheric and oceanic fluid dynamics: fundamentals and large-scale circulation* (2nd edition). Cambridge New York, NY Port Melbourne Delhi Singapore: Cambridge University Press.

Veiga, J. A. P., Pezza, A. B., Simmonds, I., & Dias, P. L. S. (2008). An analysis of the environmental energetics associated with the transition of the first South Atlantic hurricane. *Geophysical Research Letters*, *35*(15). https://doi.org/10.1029/2008GL034511

Velasco, I., & Fritsch, J. M. (2012). Mesoscale convective complexes in the Americas. *Journal of Geophysical Research: Atmospheres*, 9591–9613. https://doi.org/10.1029/JD092iD08p09591@10.1002/(ISSN)2169-8996.RAINFALL1

Wang, B., Liu, F., & Chen, G. (2016). A trio-interaction theory for Madden–Julian oscillation. *Geoscience Letters*, *3*(1), 34. https://doi.org/10.1186/s40562-016-0066-z

Wang, Z. (2012). Thermodynamic Aspects of Tropical Cyclone Formation. *Journal of the Atmospheric Sciences*, *69*(8), 2433–2451. https://doi.org/10.1175/JAS-D-11-0298.1

Wang, Z., Montgomery, M. T., & Dunkerton, T. J. (2010). Genesis of Pre–Hurricane Felix (2007). Part I: The Role of the Easterly Wave Critical Layer. *Journal of the Atmospheric Sciences*, *67*(6), 1711–1729. https://doi.org/10.1175/2009JAS3420.1

Wing, A. A., Camargo, S. J., & Sobel, A. H. (2016). Role of Radiative–Convective Feedbacks in Spontaneous Tropical Cyclogenesis in Idealized Numerical Simulations. *Journal of the Atmospheric Sciences*, *73*(7), 2633–2642. https://doi.org/10.1175/JAS-D-15-0380.1

Wing, A. A., Emanuel, K. A., Holloway, C. E., & Muller, C. J. (2018). Convective Self-Aggregation in Numerical Simulations: A Review. In R. Pincus, D. Winker, S. Bony, & B. Stevens (Eds.), *Shallow Clouds, Water Vapor, Circulation, and Climate Sensitivity* (pp. 1–25). Cham: Springer International Publishing. https://doi.org/10.1007/978-3-319-77273-8_1

Yang, D. (2018a). Boundary Layer Diabatic Processes, the Virtual Effect, and Convective Self-Aggregation. *Journal of Advances in Modeling Earth Systems*, *10*(9), 2163–2176. https://doi.org/10.1029/2017MS001261

Yang, D. (2018b). Boundary Layer Height and Buoyancy Determine the Horizontal Scale of Convective Self-Aggregation. *Journal of the Atmospheric Sciences*, *75*(2), 469–478. https://doi.org/10.1175/JAS-D-17-0150.1

Yang, D. (2019). Convective Heating Leads to Self-Aggregation by Generating Available Potential Energy. *Geophysical Research Letters*, *0*(ja). https://doi.org/10.1029/2019GL083805

Yang, D., & Ingersoll, A. P. (2013). Triggered Convection, Gravity Waves, and the MJO: A Shallow-Water Model. *Journal of the Atmospheric Sciences*, *70*(8), 2476–2486. https://doi.org/10.1175/JAS-D-12-0255.1

Yang, D., & Ingersoll, A. P. (2014). A theory of the MJO horizontal scale. *Geophysical Research Letters*, *41*(3), 1059–1064. https://doi.org/10.1002/2013GL058542

Zhang, F., & Emanuel, K. A. (2016). On the Role of Surface Fluxes and WISHE in Tropical Cyclone Intensification. *Journal of the Atmospheric Sciences*, *73*(5), 2011–2019. https://doi.org/10.1175/JAS-D-16-0011.1

Zhou, W., Held, I. M., & Garner, S. T. (2013). Parameter Study of Tropical Cyclones in Rotating Radiative–Convective Equilibrium with Column Physics and Resolution of a 25-km GCM. *Journal of the Atmospheric Sciences*, *71*(3), 1058–1069. https://doi.org/10.1175/JAS-D-13-0190.1

Figures

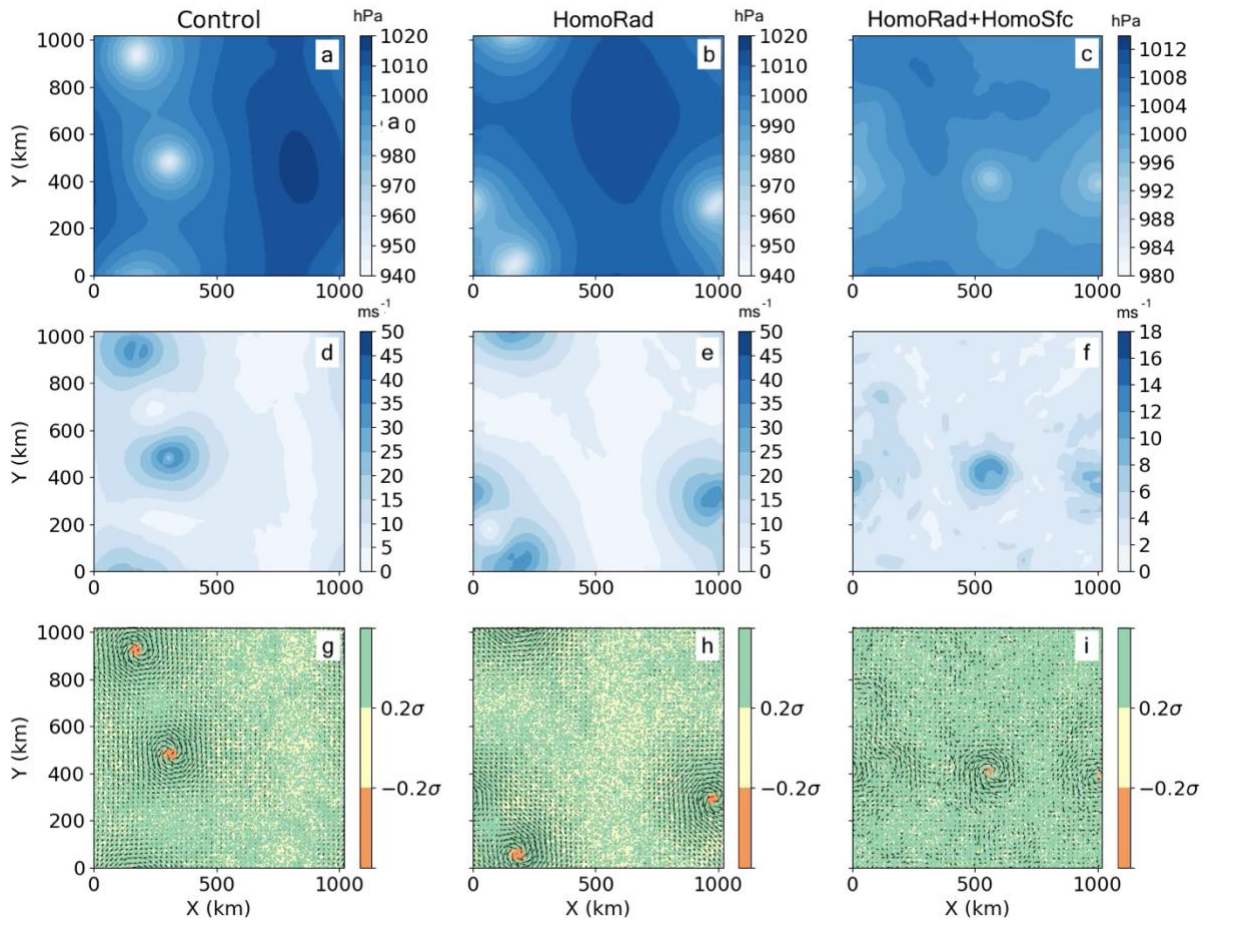

Figure 1. Map views of surface pressure, surface wind speed and OW at z = 2 km at t = 60 days. (a-c) contours of surface pressure (hPa), (d-f) and surface wind speed (m/s) and (g-i) OW (showing regions where OW is less than -0.2 times the spatial standard deviation, between -0.2 and 0.2 times the spatial standard deviation and larger than 0.2 times the spatial standard deviation). The first, second and third columns correspond to the Control, HomoRad and HomoRad+HomoSfc simulations, respectively.

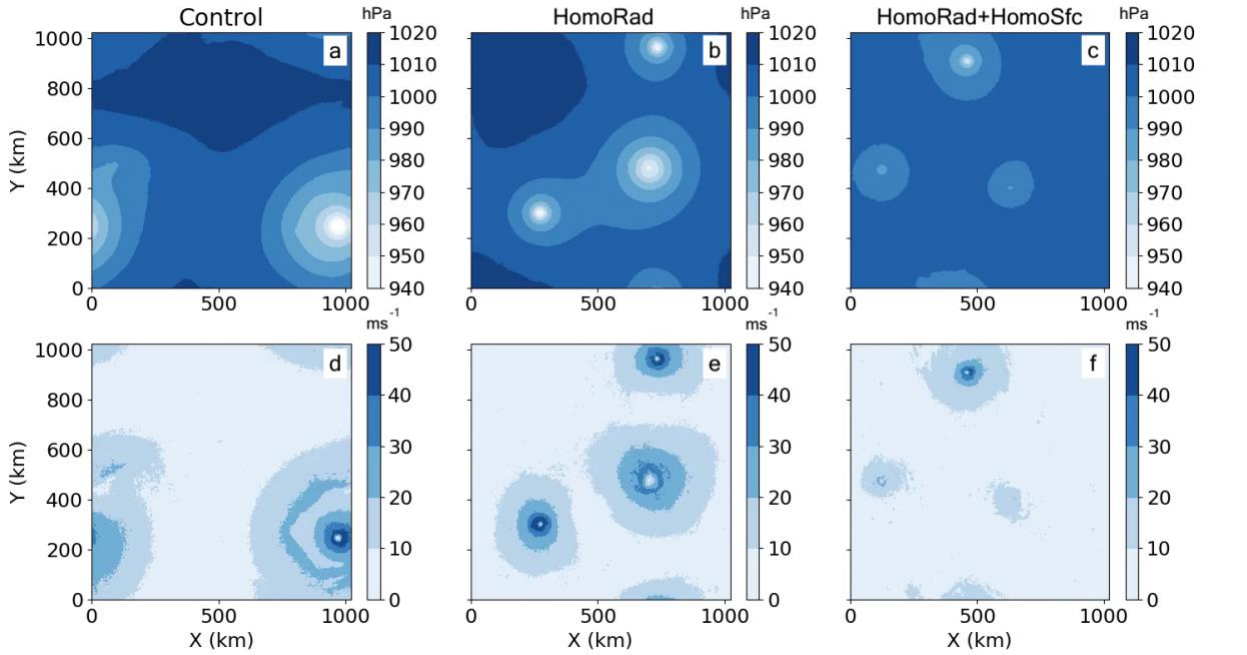

Figure 2. Map views of surface pressure and surface wind speed at t = 60 days for simulations with 2-km resolution. (a-c) contours of surface pressure (hPa) and (d-f) and surface wind speed (m/s). The first, second and third columns correspond to the Control, HomoRad and HomoRad+HomoSfc simulations, respectively.

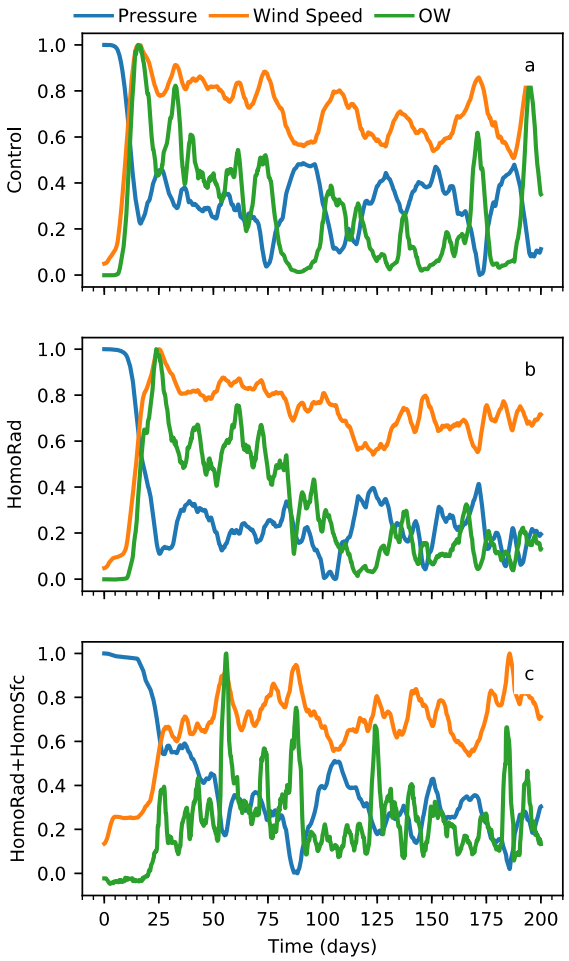

Figure 3. Time evolution of maximum surface wind speed, minimum surface pressure, and minimum OW at z = 2 km. (a) Corresponds to the Control simulation, (b) corresponds to the HomoRad simulation and (c) corresponds to the HomoRad+HomoSfc simulation. In (a-c) blue represents the minimum surface pressure scaled as $P_{scaled}(t) = \frac{P_{min}(t) - \min(P_{min})}{\max(P_{\min}) - \min(P_{\min})}$, orange represents the maximum wind speed scaled as $V_{scaled}(t) = \frac{|V_{max}(t)|}{\max(V_{max})}$ and green represents the minimum Okubo-Weiss parameter scaled as $OW_{scaled}(t) = \frac{OW_{min}(t)}{\min(OW_{min})}$, where the subscript *min* denotes spatial minimum, and the functions max(A) and min(A) take the maximum and the minimum of the field A over time, respectively.

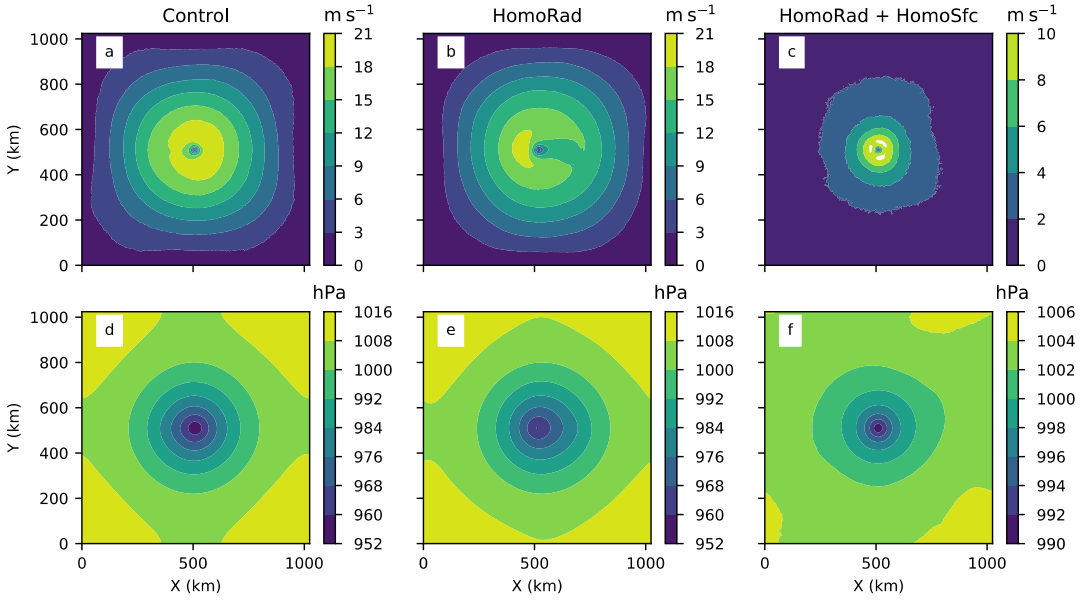

Figure 4. Map views of surface wind speed and surface pressure in the composite TCs. (a-c) contours of surface wind speed (m/s). (d-f) surface pressure (hPa). The first, second and third columns correspond to the Control, HomoRad and HomoRad+HomoSfc simulations, respectively.

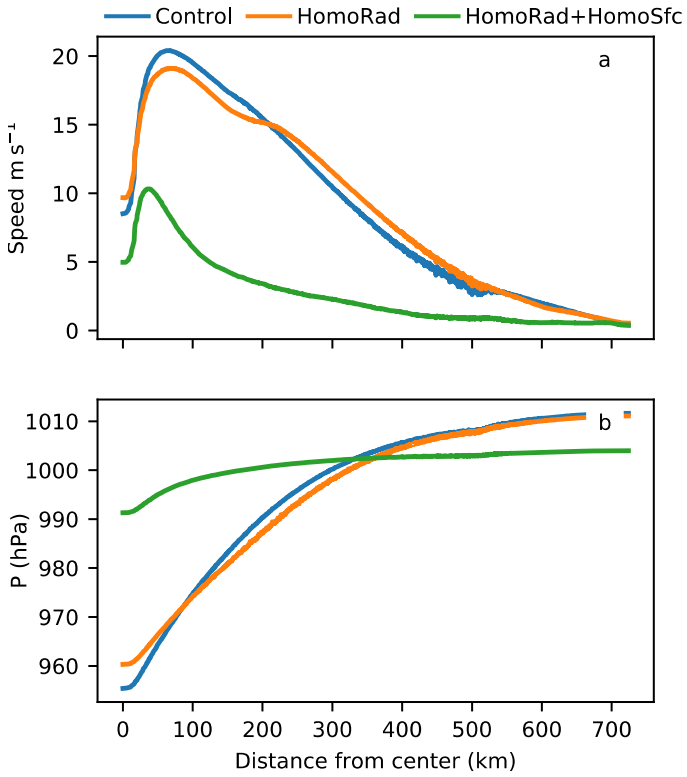

Figure 5. Radial structure of maximum wind speed at the surface and minimum surface pressure in the composite TCs. (a) Maximum surface wind speed (m/s). (b) Minimum surface pressure (hPa). Blue corresponds to the Control simulation, orange corresponds to the HomoRad simulation, and green corresponds to the HomoRad+HomoSfc simulation.

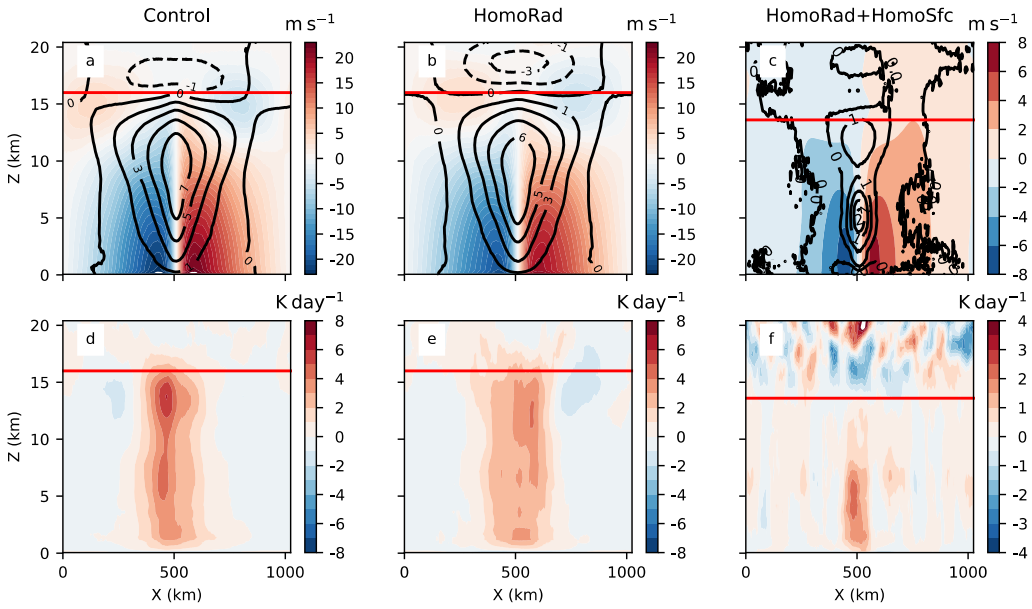

Figure 6. Horizontal – vertical cross sections of tangential wind speed, temperature anomaly and convective heating rate in the composite TC. (a-c) colored contours of tangential wind speed (m/s) and black contours of temperature anomaly (K). (d-f) colored contours of convective heating rate (K/day) and a red line indicating the height of the tropopause defined by zero radiative cooling rate. The first, second and third columns correspond to the Control, HomoRad and HomoRad+HomoSfc simulations, respectively. All represented fields are at y = 512 km

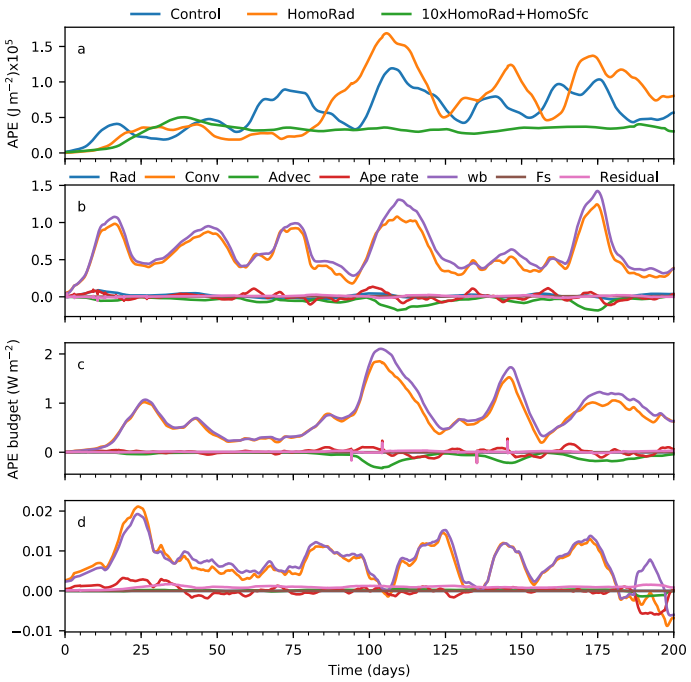

Figure 7. The available potential energy (APE) and its budget, integrated from the surface to 15 km. (a) The APE in the Control, HomoRad and HomoRad+HomoSfc experiments. APE of HomoRad+HomoSfc is multiplied by 10 to highlight features. (b) The APE budgets for the Control simulation. (c) The APE budgets for the HomoRad simulation. (d) The APE budgets for the HomoRad+HomoSfc simulation. In (b-d), red represents the total APE change rate, blue represents the radiation term, orange represents the convection term, green represents the advection term, purple represents the conversion term ,brown represents the surface fluxes term and pink represents the residual.

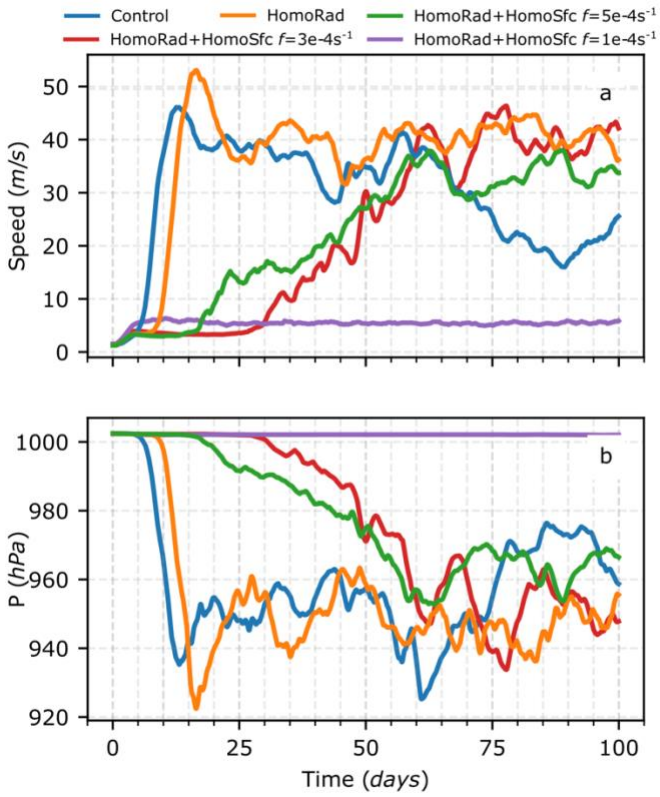

Figure 8. Time evolution of maximum surface wind speed and minimum surface pressure for simulations at 2-km resolution. (a) Shows wind speed (m s^{-1}), (b) shows minimum surface pressure (hPa). Different lines correspond to different experiments (see legend).